Supporting Information

Efficient Tandem and Triple-Junction Polymer Solar Cells

Weiwei Li, Alice Furlan, Koen H. Hendriks, Martijn M. Wienk, René A. J. Janssen*

Molecular Materials and Nanosystems, Eindhoven University of Technology, P.O. Box 513, 5600 MB Eindhoven, The Netherlands. *E-mail: r.a.j.janssen@tue.nl*

1. Materials and General Methods

Materials. All synthetic procedures were performed under argon atmosphere. Commercial chemicals were used as received. Dry solvents were distilled over 4 Å molecular sieves. [60]PCBM (purity 99%) and [70]PCBM (purity ~95%) were purchased from Solenne BV. 4-methylthiophene-2-carbonitrile (**1**)[S1] and poly[(9,9-dioctyl-2,7-fluorene)-*alt*-(9,9-bis(3'-(*N,N*-dimethylamine)propyl)-2,7-fluorene)] (PFN)[S2] were synthesized according to literature procedures.

Methods. ^{1}H-NMR and ^{13}C-NMR spectra were recorded at 400 MHz and 100 MHz on a VARIAN mercury spectrometer with $CDCl_3$ as the solvent and tetramethylsilane (TMS) as the internal standard. Molecular weight was determined with GPC at 80 °C on a PL-GPC 120 system using a PL-GEL 5μm MIXED-C column and *o*-DCB as the eluent against polystyrene standards. Optical absorption spectra were recorded on a PerkinElmer Lambda 900 UV/vis/nearIR spectrophotometer. Cyclic voltammetry was conducted with a scan rate of 0.1 V s^{-1} under an inert atmosphere with 1 M tetrabutylammonium hexafluorophosphate in *o*-DCB as the electrolyte. The working electrode was a platinum disk and the counter electrode was a silver electrode. A silver wire coated with silver chloride (Ag/AgCl) was used as quasi-reference electrode in combination with Fc/Fc+ as an internal standard. The concentration of the sample in the electrolyte was approximately 1 mM, based on monomers.

2. Synthesis of PMDPP3T

Reaction route. Polymer PMDPP3T was synthesised according to Scheme S1.

Scheme S1. Synthesis Route of DPP-Based Monomer and PMDPP3T[a]

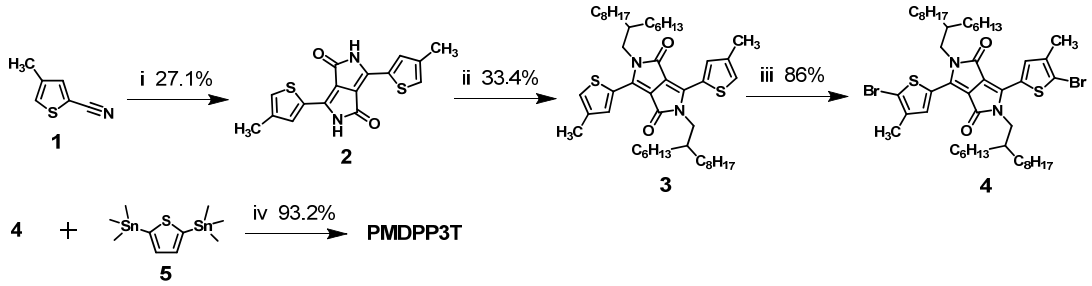

[a] Reaction conditions: (i) sodium/$FeCl_3$ in 2-methyl-2-butanol at 95 °C, 2 h; **1** was added and diethyl succinate was added dropwise at 120 °C; reflux at 120 °C, 3 h; (ii) K_2CO_3,18-crown-6, and 2-hexyldecyl bromide in DMF at 120 °C, 16 h; (iii) NBS in $CHCl_3$; (iv) Stille polymerization to PMDPP3T using $Pd_2(dba)_3/PPh_3$ in toluene/DMF (10:1, v/v) at 115 °C.

3,6-Bis(4-methylthiophene-2-yl)pyrrolo[3,4-*c*]pyrrolo-1,4(2*H*,5*H*)-dione (2). Sodium (0.86 g, 37.3 mmol) and iron(III) chloride (10 mg) were added into 2-methyl-2-butanol (10 mL) and the mixture was heated to 95 °C for 2 h until the sodium dissolved. After the solution was cooled to 75 °C, 4-methylthiophene-2-carbonitrile (**1**) (1.84 g, 14.9 mmol) was added and the mixture was heated to reflux. Diethyl succinate (1.82 g, 10.5 mmol) in 2-methyl-2-butanol (10 mL) was added dropwise in 30 min. After stirring for 3 h, the reaction was cooled to 50 °C, and methanol (10 mL) and glacial acetic acid (10 mL) were added. The mixture was then refluxed for 30 min., cooled to room temperature, and poured into methanol (100 mL). The precipitate was filtered and washed with water and methanol to afford **2** as dark red solid (1.33 g, 27.1%), which was used without further purification.

2,5-Bis(2-hexyldecyl)-3,6-bis(4-methylthiophen-2-yl)pyrrolo[3,4-*c*]pyrrole-1,4(2*H*,5*H*)-dione (3). To a solution of **2** (1.33 g, 4.05 mmol), potassium carbonate (1.68 g, 12.1 mmol) and 18-crown-6 (20 mg) in DMF (30 mL) was added 2-hexyldecyl bromide (3.09 g, 10.1 mmol). The reaction mixture was stirred at 120 °C for 16 h and then cooled to room temperature. Diethyl ether (100 mL) and water (100 mL) were added and the layers were separated. The organic layer was washed with brine and the solvent evaporated. The resulting solid was subjected to column chromatography (silica, eluent heptane/CH_2Cl_2, 75%/25%) to afford **3** (1.05 g, 33.4%) as red solid. ^{1}H NMR δ (ppm): 8.68 (s, 2H), 7.21 (s, 2H), 4.00 (d,

4H), 2.37 (s, 6H), 1.91 (m, 2H), 1.60−1.20 (m, 48H), 0.86 (m, 12H). ^{13}C NMR δ (ppm): 161.77, 140.29, 139.14, 137.11, 129.52, 126.48, 107.74, 46.17, 37.68, 31.88, 31.77, 31.21, 29.30, 22.67, 22.63, 15.62, 14.11, 14.08. MS (MALDI): calculated: 777.26, found: 776.52 (M^+).

3,6-Bis(5-bromo-4-methylthiophen-2-yl)-2,5-bis(2-hexyldecyl)pyrrolo[3,4-*c*]pyrrole-1,4(2*H*,5*H*)-dione (4). To a degassed solution of **3** (0.777 g, 1 mmol) in chloroform (20 mL) at 0 ^{o}C, *N*-bromosuccinimide (0.356 g, 2 mmol) was added in portions, and the reaction mixture was stirred for 24 h at room temperature. Then the reaction mixture was heated to 50 ^{o}C and stirred for another 24 h to ensure the full conversion of **3** to **4**. After this the mixture was diluted with chloroform, washed with water and brine, and evaporated. The resulting solid was dissolved in chloroform (5 mL) and precipitated into methanol (100 mL) to yield **4** (0.80 g, 86%) as a purple solid. ^{1}H NMR δ (ppm): 8.56 (s, 2H), 3.91 (d, 2H), 2.29 (s, 6H), 1.88 (m, 2H), 1.60−1.20 (m, 48H), 0.86 (m, 12H). ^{13}C NMR δ (ppm): 161.47, 139.40, 139.09, 136.48, 128.96, 116.71, 107.85, 46.30, 37.73, 31.89, 31.77, 29.52, 29.30, 22.68, 22.63, 15.19, 14.12, 14.09. MS (MALDI): calculated: 935.05, found: 934.38 (M^+).

Poly[[2,5-bis(2-hexyldecyl)-2,3,5,6-tetrahydro-3,6-dioxopyrrolo[3,4-c]pyrrole-1,4-diyl]-*alt*-[3',3''-dimethyl-2,2':5',2''-terthiophene]-5,5''-diyl] (PMDPP3T). To a degassed solution of monomer **4** (72.53 mg, 0.078 mg), 5,5'-bis(trimethylstannyl)thiophene (**5**) (31.79 mg, 0.078 mmol) in toluene (3 mL) and DMF (0.3 mL), tris(dibenzylideneacetone)-dipalladium(0) (2.13 mg, 2.3 μmol) and triphenylphosphine (2.44 mg, 9.3 μmol) were added. The mixture was stirred at 115 °C for 18 h, after which it was precipitated in methanol and filter through a Soxhlet thimble. The polymer was extracted with acetone, hexane, dichloromethane and chloroform. The chloroform fraction was evaporated and the polymer was precipitated in acetone. The polymer was collected by filtering over a 0.45 μm PTFE membrane filter and dried in a vacuum oven to yield PMDPP3T (62 mg, 93.2%) as a dark solid. ^{1}H NMR δ (ppm): 8.94 (b, 2H), 7.10 (b, 2H), 4.04 (b, 4H), 2.50 (b, 6H), 1.97 (b, 2H), 1.20 (b, 48H), 0.80 (b, 12H).

3. Device Preparation and Characterisation

Field-effect transistors. FETs were fabricated using heavily doped silicon wafers as the common gate electrode with a 200 nm thermally oxidized SiO_2 layer as the gate dielectric. Using conventional photolithography, gold source and drain electrodes were defined in a bottom contact device configuration with a channel width and length of 1 cm and 10 μm, respectively. A 10 nm layer of titanium was used, acting as an adhesion layer for the gold on SiO_2. The SiO_2 layer was exposed to the vapour of the primer hexamethyldisilazane for 60 min. prior to semiconductor deposition to passivate the surface of the dielectric. Polymer films were spun from a chloroform solution (3 mg mL^{-1}) at 3000 rpm for 30 s. Freshly prepared devices were annealed in a dynamic vacuum of 10^{-5} mbar at 150 °C for 12 h to remove traces of the solvent. All electrical measurements were performed in vacuum using an HP 4155C semiconductor parameter analyzer.

Single-junction solar cells. Single-junction photovoltaic devices were made by spin coating poly(3,4-ethylenedioxythiophene):poly(styrene sulfonate) (PEDOT:PSS) (Clevios P, VP AI 4083) onto pre-cleaned, patterned indium tin oxide (ITO) substrates in air (14 Ω per square) (Naranjo Substrates). The PMDPP3T-fullerene photoactive layers were deposited by spin coating in air from a chloroform solution containing the polymer and [60]PCBM or [70]PCBM with different content ratio and the appropriate amount of *o*-DCB. LiF (1 nm) and Al (100 nm) were deposited by vacuum evaporation at ~2×10^{-7} mbar as the back electrode. For the devices based on PFN/Al, PFN solution in methanol with 0.25% acetic acid was spin coated on the top of active layer (5 nm), followed by depositing Al (100 nm) by vacuum evaporation at ~2×10^{-7} mbar. The active area of the cells was 0.090 or 0.160 cm^2, which provided similar results. For application of the PCDTBT:[70]PCBM active layer the PEDOT:PSS layer was dried by heating at 140 °C for 10 minutes. On top of the dried PEDOT:PSS a mixture of PCDTBT and [70]PCBM in a 1:4 ratio from 30% chlorobenzene in *o*-DCB using a polymer concentration of 7 mg mL^{-1}, was cast in nitrogen atmosphere. The PCDTBT active layer was dried on a hotplate for 10 minutes at 70 °C.

Optical and electrical modelling. Prediction of the performance of tandem and triple-junction cells was carried out as described earlier.[S3] In short: For a series of single-junction cells the performance as a function of photoactive layer thickness was determined. From these data the internal quantum efficiency and the shape of the $J-V$ as a function of layer thickness were extracted. Optical modelling using the transfer matrix formalism with a

commercial software package SETFOS 3 (Fluxim) combined with the IQE data provides the current generation capacity in each sub-cell, depending on the exact layout of the optical stack. Combining these current generation capacities with the relevant $J-V$ shape and adding the sub-cell $J-V$'s according Kirchhoff's law provides the $J-V$ characteristics for the tandem for any given thickness combination. The optical parameters of PMDPP3T:[60]PCBM blends for these calculations were determined from reflection/transmission measurement on active layers on quartz. The optical data for PCDTBT:[70]PCBM were obtained from Ref. S4. The results for the tandem cell are shown in Figure S8.

Multi-junction solar cells. Tandem and triple-junction solar cells were obtained by solution processing an intermediate contact consisting of ZnO nanoparticles[S5] and PEDOT:PSS on the PCDTBT:[70]PCBM active layer that was prepared as described above for single-junction cells. The ZnO layer was spun in nitrogen atmosphere from a solution of 10 mg mL^{-1} ZnO nanoparticles in isopropanol. The pH neutral PEDOT:PSS (Orgacon, Agfa) was diluted 1:1 with ultrapure water after which 0.2 mL mL^{-1} isopropanol was added to improve the wetting on the ZnO nanoparticles. Prior to spin casting in air the solution was filtered using a 5.0 μm Whatman Puradisc FP30 syringe filter. The PMDPP3T:[60]PCBM active layer was spun on top of the pH neutral PEDOT:PSS in air. For triple-junction cells the procedure was repeated, starting with spin coating ZnO nanoparticles in nitrogen atmosphere on the on the PMDPP3T:[60]PCBM active layer. Finally a back contact of 1 nm LiF and 100 nm Al was evaporated in vacuum for all devices. Device areas of 0.09 and 0.16 cm^2 were used, which provided similar results.

External quantum efficiency. EQE measurements were done in a homebuilt set-up, with the devices kept in a nitrogen filled box with a quartz window and illuminated through an aperture of 2 mm. Mechanically modulated (Stanford Research, SR 540) monochromatic (Oriel, Cornerstone 130) light from a 50 W tungsten halogen lamp (Osram 64610) was used as probe light, in combination with continuous bias light from a solid state laser (B&W Tek Inc. 532 nm, 30 mW and 780 nm, 21 mW). The intensity of the bias laser light was adjusted using a variable-neutral density filter. The response was recorded as the voltage over a 50 Ω resistance, using a lock-in amplifier (Stanford Research Systems SR 830). For all the single-junction devices and the PMDPP3T:[60]PCBM subcell, the measurement was carried out under representative illumination intensity (AM1.5G equivalent, provided by the 532 nm-laser). For the PCDTBT:[70]PCBM subcell, the measured EQE was mathematically

corrected for the intensity difference between the monochromatic light and AM1.5G. For the tandem subcells, a compensating electrical bias was applied by the lock-in amplifier to ensure short-circuit conditions in the respective subcells during the spectral response measurements. More details can be found in Refs. S6-S8.

Current-density – voltage characteristics. *J*−*V* curves were measured under simulated solar light (100 mW cm^{-2}) from a tungsten–halogen lamp filtered by a Hoya LB100 daylight using a Keithley 2400 source meter. No mismatch correction was done. For the single-junction cells the accurate short-circuit current density (J_{sc}) was determined from the EQE by convolution with the AM1.5G solar spectrum. For the tandem and triple-junction solar cell measurements, the simulated solar light spectrum was tuned to provide appropriate illumination to each subcell. This was achieved by adjusting the voltage over the tungsten halogen lamp and the distance to the sample in such a way that both the wide bandgap and the narrow bandgap single-junction reference cell gave the exact J_{sc} as determined from the EQE measurement. The *J*−*V* curves of the tandem and triple-junction solar cells were measured under illumination through a mask of identical dimensions to the device area determined by the overlap of the ITO and Al electrodes, to avoid extra current generation due to the high lateral conductivity of the pH neutral PEDOT:PSS.[S9]

Detailed comparison of PDPP3T and PMDPP3T. Since our first report on PDPP3T (PCE = 4.7%)[S10] there have been improvements related to the synthesis and molecular weight. Recently, Ye *et al.* reported PCE = 6.7% for PDPP3T.[S11] In the course our research, we also succeeded in an improved synthesis of PDPP3T (identical route to the one used now to make PMDPP3T) to reach PCE = 7.1%. These changes are mainly due to improvements in molecular weight and better morphologies in blends with [70]PCBM. In Table S1 we collect the relevant data on PDPP3T solar cells and compare these to the new PMDPP3T. As can be seen the PCE of PMDPP3T is similar to the more recent versions of PDPP3T, but does give an enhanced EQE response at long wavelengths, especially when using [60]PCBM. This is crucial advantage for a material as the near infrared absorber for a multi-junction cell. Figure S1 below shows the important increase at 800 nm that makes that PMDPP3T is tailored to the use in multi-junction solar cells.

Table S1. Performance of PDPP3T and PMDPP3T.

Polymer	Acceptor	M_n (kD)	J_{sc} (mA/cm^2)	V_{oc} (V)	FF (-)	PCE (%)	EQE at 800 nm (%)	Reference
PDPP3T	[70]PCBM	10	6.3	0.68	0.63	2.7	15	S10
PDPP3T	[70]PCBM	54	11.8	0.65	0.69	4.7	34	S10
PDPP3T	[70]PCBM	780	15.4	0.66	0.66	6.7	47	S11
PDPP3T	[70]PCBM	147	15.4	0.67	0.69	7.1	49	Unpublished
PMDPP3T	[70]PCBM	110	16.9	0.59	0.68	6.8	55	This work
PMDPP3T	[60]PCBM	110	14.8	0.61	0.65	5.8	61	This work

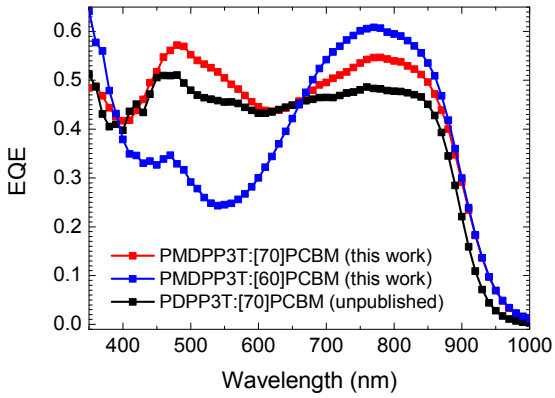

Figure S1. EQE of PMDPP3T:[70]PCBM and PMDPP3T:[60]PCBM solar cells with LiF/Al back contacts compared to the best PDPP3T:[70]PCBM devices.

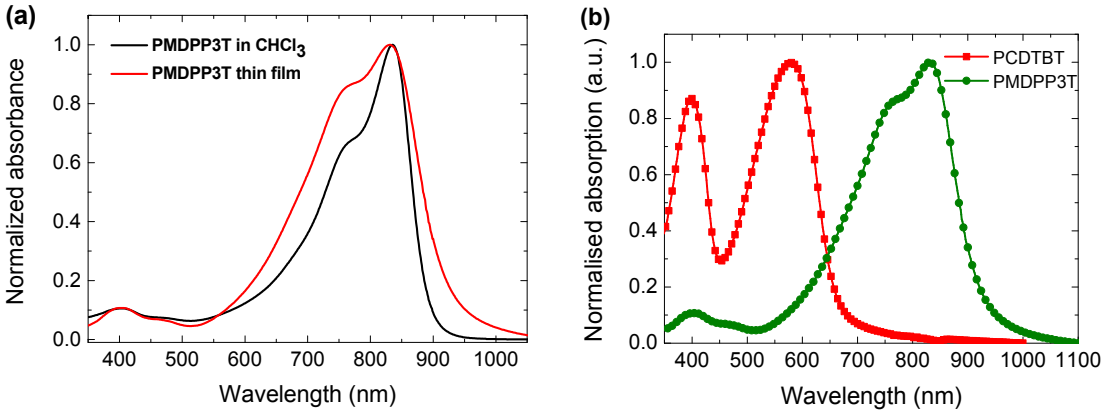

Figure S2. (a) Optical absorption spectra of the PMDPP3T in $CHCl_3$ solution and in a thin film. (b) UV-visible-near infrared absorption spectra of PMDPP3T and PCDTBT thin films showing the complementary coverage of the two optical absorbers.

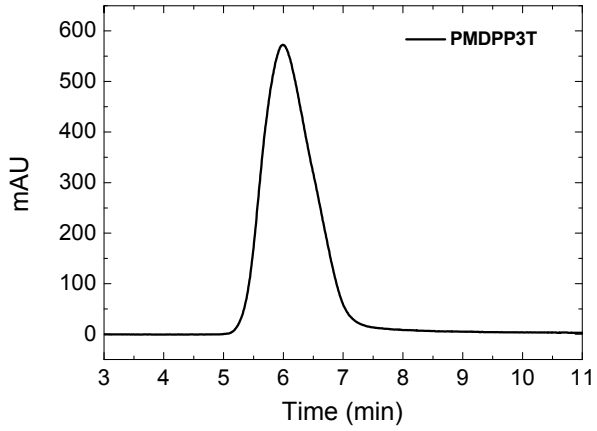

Figure S3. GPC trace of PMDPP3T with *o*-DCB as eluent at 80 °C.

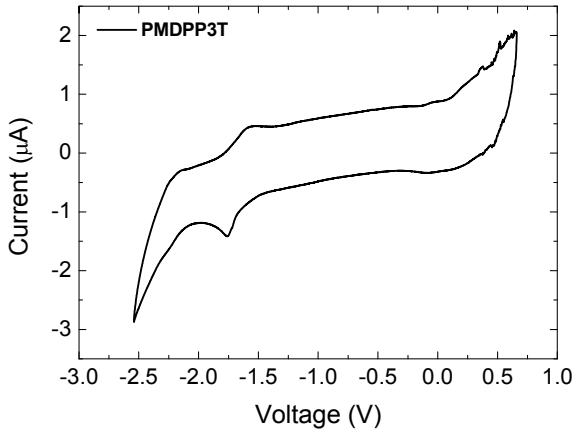

Figure S4. Cyclic voltammogram of PMDPP3T in *o*-DCB. Potential vs. Fc/Fc^{+}.

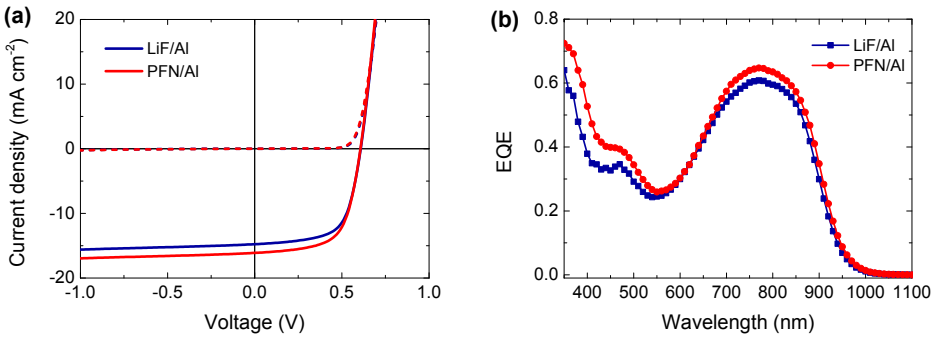

Figure S5. (a) *J*−*V* and (b) EQE of optimized single-junction PMDPP3T:[60]PCBM cells with LiF/Al and PFN/Al back contacts under simulated AM1.5G illumination.

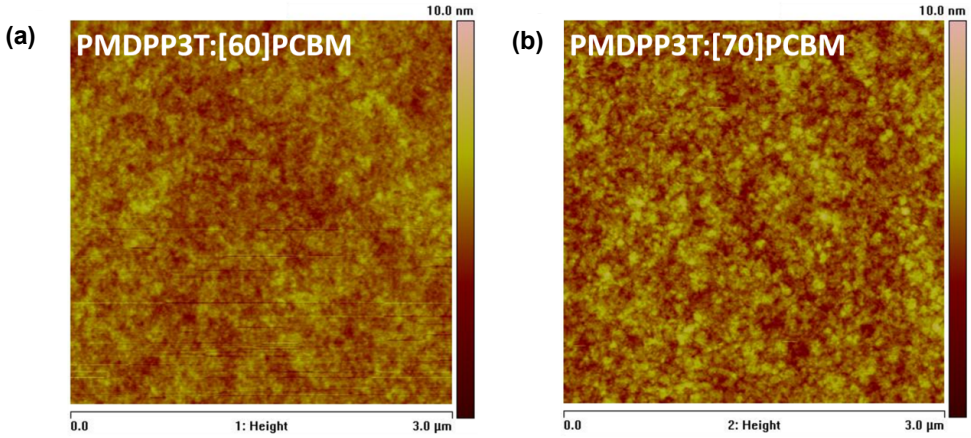

Figure S6. AFM height images of the optimized PMDPP3T:[60]PCBM (1:3 w/w) (a) and PMDPP3T:[70]PCBM (1:3 w/w) (b) films. The root mean square roughness is 0.61 and 0.81 nm, respectively.

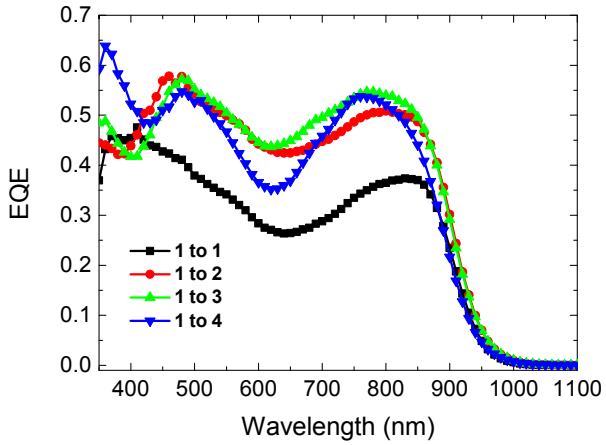

Figure S7. EQE of PMDPP3T solar cells with different weight ratio's of [70]PCBM.

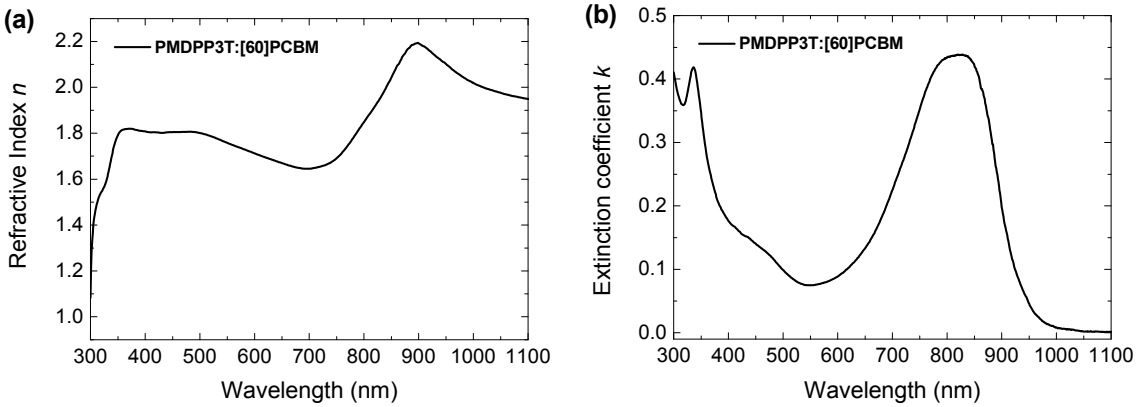

Figure S8. Refractive index (*n*) and extinction coefficient (*k*) of PMDPP3T:[60]PCBM (1:3, w/w/) layers vs. wavelength.

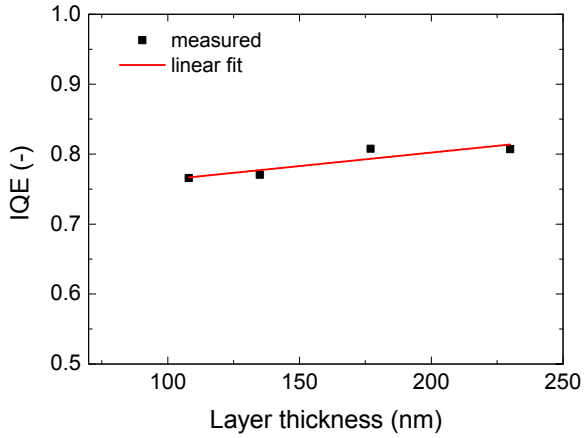

Figure S9. Internal quantum efficiency (IQE) of PMDPP3T:[60]PCBM vs. active layer thickness.

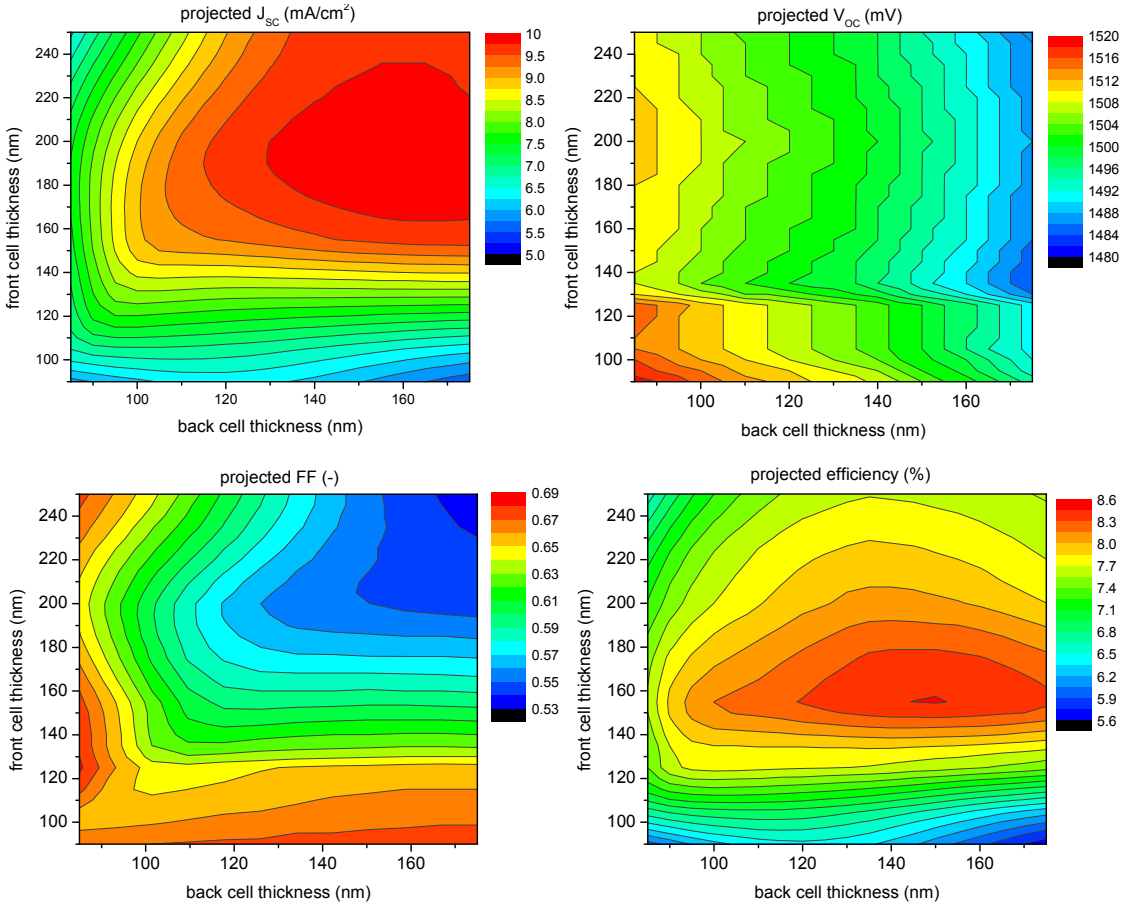

Figure S10. Predicted photovoltaic parameters for tandem cells as a function of the thicknesses of the PCDTBT:[70]PCBM front cell and the PMDPP3T:[60]PCBM back cell.

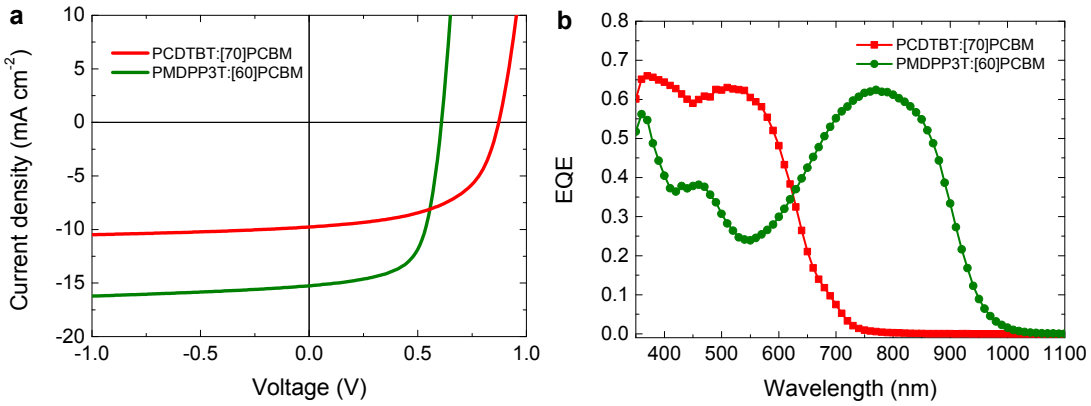

Figure S11. (a) Current density – voltage ($J-V$) characteristics and (b) spectrally resolved external quantum efficiencies (EQEs) for single-junction PCDTBT:[70]PCBM (1:4 w/w, 155 nm) and PMDPP3T:[60]PCBM (1:3 w/w, 150 nm) cells sandwiched between ITO/PEDOT:PSS and LiF/Al electrodes under simulated AM1.5G illumination with an irradiation intensity of 100 mW cm^{-2}. The layer thicknesses correspond to the thicknesses used in the optimized tandem cell.

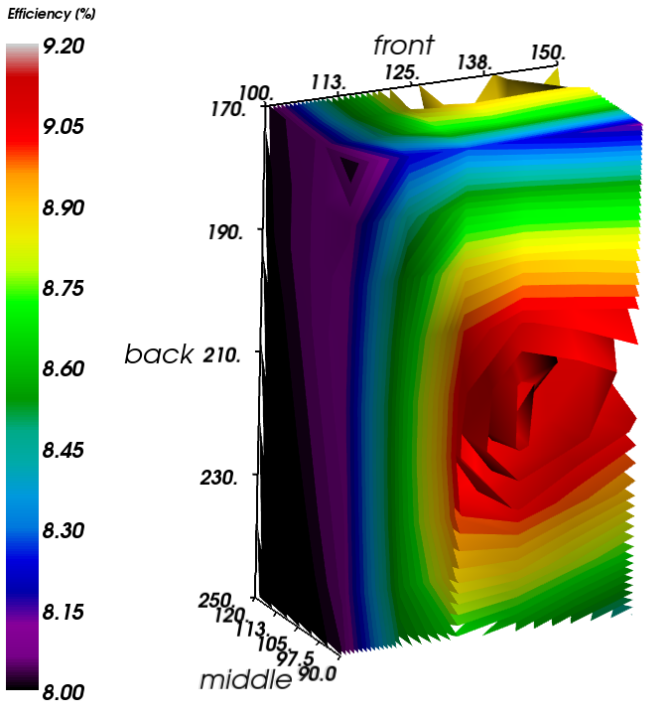

Figure S12. Predicted efficiency for triple cells as a function of the thicknesses of the PCDTBT:[70]PCBM front cell and the PMDPP3T:[60]PCBM middle and back cells.

Table S2. Summary of photovoltaic devices based on PMDPP3T with different content ratio of [70]PCBM.

Polymer	Ratio to [70]PCBM	J_{sc}[a] (mA cm^{-2})	V_{oc} (V)	FF	PCE[a] (%)	EQE_{max}[b]
PMDPP3T	1:1	11.7	0.61	0.46	3.0	0.37
PMDPP3T	1:2	16.4	0.61	0.63	6.3	0.51
PMDPP3T	1:3	16.9	0.59	0.68	6.8	0.55
PMDPP3T	1:4	15.6	0.59	0.69	6.3	0.54

[a] J_{sc} was calculated by integrating the EQE spectrum with the AM1.5G spectrum. [b] Measured in the region of polymer absorption.

Table S3. Thickness dependence of performance of PMDPP3T:[60]PCBM (1:3, w/w) solar cells.

Thickness (nm)	J_{sc}[a] (mA cm^{-2})	V_{oc} (V)	FF	PCE[a] (%)
84	9.8	0.62	0.7	4.3
108	14	0.61	0.66	5.7
135	14.8	0.61	0.65	5.8
177	15.7	0.59	0.59	5.6
230	16.9	0.58	0.56	5.5

[a] J_{sc} was calculated by integrating the EQE spectrum with the AM1.5G spectrum.

References

S1 Li, Z.; Ding, J. F.; Song, N. H.; Du, X. M.; Zhou, J. Y.; Lu, J. P.; Tao, Y. *Chem. Mater.* **2011**, *23*, 1977-1984.

S2 Huang, F.; Wu, H. B.; Wang, D.; Yang, W.; Cao, Y. *Chem. Mater.* **2004**, *16*, 708-716.

S3 Gilot, J.; Wienk, M. M.; Janssen, R. A. J. *Adv. Mater.* **2010**, *22*, E67-E71.

S4 Steirer, K. X.; Ndione, P. F.; Widjonarko, N. E.; Lloyd, M. T.; Meyer, J.; Ratcliff, E. L.; Kahn, A.; Armstrong, N. R.; Curtis, C. J.; Ginley, D. S.; Berry, J. J.; Olson, D. C. *Adv. Energy Mater.* **2011**, *1*, 813-820.

S5 Beek, W. J. E.; Wienk, M. M.; Kemerink, M.; Yang, X. N.; Janssen, R. A. J. *J. Phys. Chem. B* **2005**, *109*, 9505-9516.

S6 Gilot, J.; Wienk, M. M.; Janssen, R. A. J. *Adv. Funct. Mater.* **2010**, *20*, 3904-3911.

S7 Gilot, J.; Wienk, M. M.; Janssen, R. A. J. *Org. Electron.* **2011**, *12*, 660–665.

S8 Wehenkel, D. J.; Hendriks, K. H.; Wienk, M. M.; Janssen, R. A. J. *Org. Electron.* **2012**, *13*, 3284–3290

S9 Sista, S.; Park, M. H.; Hong, Z. R.; Wu, Y.; Hou, J. H.; Kwan, W. L.; Li, G.; Yang, Y. *Adv. Mater.* **2010**, *22*, 380-383.

S10 Bijleveld, J. C.; Zoombelt, A. P.; Mathijssen, S. G. J.; Wienk, M. M.; Turbiez, M.; de Leeuw, D. M.; Janssen, R. A. J. *J. Am. Chem. Soc.* **2009**, *131*, 16616-16617.

S11 Ye, L.; Zhang, S.; Ma, W.; Fan, B.; Guo, X.; Huang, Y.; Ade, H.; Hou, J. *Adv. Mater.* **2012**, *24*, 6335-6341.